RESEARCH ARTICLE



The pivotal role of Vulcanian activity in ending the explosive phase of rhyolitic eruptions: the case of the Big Obsidian Flow eruption (Newberry Volcano, USA)

Kathleen R. Trafton 10 · Thomas Giachetti 1

Received: 25 December 2021 / Accepted: 19 October 2022 © International Association of Volcanology & Chemistry of the Earth's Interior 2022

Abstract

Explosive volcanism produces myriad hazards from pyroclastic flows to widespread ejecta dispersal. Effusive eruptions can emit noxious, damaging gases and extensive lava flows. A single eruption of silicic magma can produce both types of activity, sometimes concurrently. Understanding what drives such eruptions, their transitions in styles, and associated hazards requires detailed observations of eruptions and analysis of resulting products. The physical and geochemical characteristics of pyroclasts serve as snapshots of final conduit processes before their egress. Here, we examine the explosive phase of the 640 CE rhyolitic eruption of Newberry Volcano (OR, USA), which began with sub-Plinian pyroclastic fallout and terminated with the effusion of the Big Obsidian Flow. To better understand shallow conduit dynamics, we combine previous work on the geochemistry and textures of obsidian pyroclasts with our detailed physical and textural analyses of > 2000 pumices from 37 layers pulled from 4 pits along the dispersal axis. We analyze the density, mass, and volume distribution of ash and lapilli layers and also examine external the texture of the latter. As with the rhyolitic eruptions of Volcán Chaitén in 2008 and Cordón Caulle in 2011–2012 (both in Chile), we find transitory Vulcanian pulses to be the link between the initial Subplinian phase and subsequent effusive activity. We also concur with recent studies that the syn-eruptive formation of obsidian by ash agglomeration and sintering along the conduit edges above the fragmentation level modulates eruptive style, ultimately leading to the subaerial effusion of rhyolitic lava.

Keywords Explosive eruptions · Explosive-effusive transition · Rhyolite · Pumice · Obsidian · Pyroclasts · Sintering

Introduction

The style of eruptions of silicic magma has often been considered through the binary lens of explosive or effusive, wherein the two are irreconcilable endmember behaviors (Eichelberger et al. 1986; Jaupart and Allègre 1991). Explosive eruptions rapidly eject freshly fragmented, bubbly magma that cools into pyroclasts in the atmosphere. Such

Editorial responsibility: U. Kueppers; Deputy Executive Editor: J. Tadeucci

This paper constitutes part of a topical collection: What pyroclasts can tell us

⊠ Kathleen R Trafton kathytrafton@gmail.com

Published online: 07 November 2022

eruptions produce notable hazards from deadly pyroclastic flows to widespread ejecta dispersal (Cioni et al. 2015) with potentially global economic and climatic consequences. Effusive eruptions, the classically more quiescent counterpart, slowly outpour degassed, generally cohesive lava. Such eruptions can not only cause local property damage but also emit toxic and environmentally-damaging gases (Baxter and Horwell 2015). The study of each eruption style's resulting products has offered invaluable insights into conduit processes, allowing for a better constraint of such hazards (Cassidy et al. 2018, and references therein). For example, characterizing pyroclasts' physical (e.g., Clarke et al. 2007; Mueller et al. 2011; Larue et al. 2013; Janebo et al. 2018; Davies et al. 2021; Trafton and Giachetti 2021) and geochemical (e.g., Rust and Cashman 2007; Cassidy et al. 2015; Watkins et al. 2017; Giachetti et al. 2020) signatures gives snapshots of near-fragmentation magma degassing and outgassing dynamics.



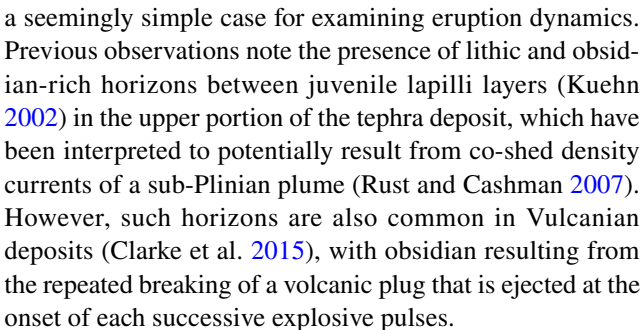
Earth Sciences Department, University of Oregon, Eugene, OR, USA

Eruptions of Volcán Chaitén in 2008 (Chile; Castro and Dingwell 2009) and Cordón Caulle in 2011–2012 (Chile; Schipper et al. 2013, 2021) are the only observed rhyolitic eruptions since the advent of modern volcanology. Both eruptions exhibited protracted hybrid explosive-effusive behavior between the explosive onset and the effusive closure of the eruption. These recent observations show that eruptive style is much less a binary and more so a spectrum, with the potential for contemporaneous explosive-effusive behavior. Furthermore, recent studies have shown that the classical idea that fragmentation is solely tied to explosive behavior may not be true; fragmentation may be necessary for the production of both explosive (pyroclasts) and effusive (lava) output (Wadsworth et al. 2020).

Obsidian pyroclasts are dense, lava-like products found in pyroclastic fallout deposits (1340 CE Mono Craters eruption, CA, USA; Gardner et al. 2017). They result from the agglomeration and sintering of ash particles primarily fragmented at depth; as a result, they can have juxtaposed, variably bubbleand volatile-rich domains that reflect the history of individual particles (Gardner et al. 2017; Watkins et al. 2017). Obsidian pyroclasts without these domains may still be formed in this way; however, they simply had enough time to sinter to homogenization (Gardner et al. 2017; Watkins et al. 2017). These pyroclasts are evidence that dense magma can build up on conduit margins despite rapid excavation during explosive eruptions. What happens if, as an eruption wanes, ash agglutinates faster than it is eroded? Dense magma could accumulate, begin filling the conduit, and potentially effuse as lava while explosions continue. Based on diffusion models of ash degassing, particle aggregation experiments, and timescales of sintering, this process is feasible (Wadsworth et al. 2020).

Should dense magma significantly build up, it may fill the conduit and prevent future explosions. As such, hybrid activity could signal a likely transition to the final effusive activity. Most silicic explosive eruptions, and particularly crystalpoor silicic eruptions, do transition to pulsatory behavior before final lava extrusion (e.g., 550 B.P. Inyo volcanic chain, CA, U.S.A., Castro and Gardner 2008; Novarupta 1912, AK, U.S.A., Nguyen et al. 2014; Ogburn et al. 2015; Cassidy et al. 2018). For example, the 2011–2012 rhyolitic eruption of Cordón Caulle began highly explosively with > 14-km-high Plinian columns on June 4th. The eruption switched to sub-Plinian/Vulcanian activity, and hybrid activity began on June 15th with contemporaneous lava effusion (Schipper et al. 2013).

In this study, we examine the 640 CE eruption of Newberry Volcano (central Oregon, USA; Fig. 1), which began explosively, producing the Newberry Pumice fallout deposit, and terminated effusively with the Big Obsidian Flow. With only one transition from explosive to effusive behavior documented and well-preserved deposits, this eruption serves as



Past studies of the Newberry Pumice fallout deposit examined clast size and distribution (Gardner et al. 1998), geochemistry (Kuehn 2002; Rust and Cashman 2007; Di Genova et al. 2017), tephrochronology (Kuehn 2002), and textures of obsidian pyroclasts (Rust and Cashman 2007). However, detailed textural analyses of the pumice that comprises > 95 wt% of the fallout (Rust and Cashman 2007) have yet to be done. To fill this gap, we analyze 37 layers of ash and lapilli for density, mass, and volume distribution, and also examine the external texture of the lapilli. We do these analyses for 4 pits roughly along the main dispersal axis of the Newberry Pumice. We then combine our results with those of previous authors (MacLeod et al. 1995; Kuehn 2002; Rust and Cashman 2007) to examine how the 640 CE eruption of the Newberry volcano eruption transpired. Ultimately, we contextualize our model of the explosive-effusive transition with those of the greater community (Cassidy et al. 2018; Wadsworth et al. 2020) and assess Vulcanian behavior as a potential link between explosive and effusive activity during rhyolitic eruptions.

Geologic setting

Locality

Newberry Volcano (central Oregon, U.S.A) is a shield-shaped volcanic complex that lies slightly east of the Cascade volcanic arc at the intersection of the Walker, Brothers, and Sisters fault zones (Fig. 1a; Walker and MacLeod 1991; Jordan et al. 2004). Newberry results from either hot spot (Xue and Allen 2006) or, as more recently proposed, subduction-related volcanism (Till et al. 2013). It erupts every ~ 1000 years (Gardner et al. 1998) and is classified as a very high-threat volcano by the United States Geological Survey (Ewert et al. 2018). Tomographic imaging of the underlying structure reveals a likely magma chamber 3–5 km below the surface (Heath et al. 2015).

Newberry has produced myriad and varied eruptions, both in terms of volume and magma composition. It is the second-most voluminous volcano in the Cascades (~500 km³) after Medicine Lake Volcano (CA) and has over 400 volcanic vents and cones (Donnelly-Nolan et al. 2011). It



Bulletin of Volcanology (2022) 84:104 Page 3 of 18 104

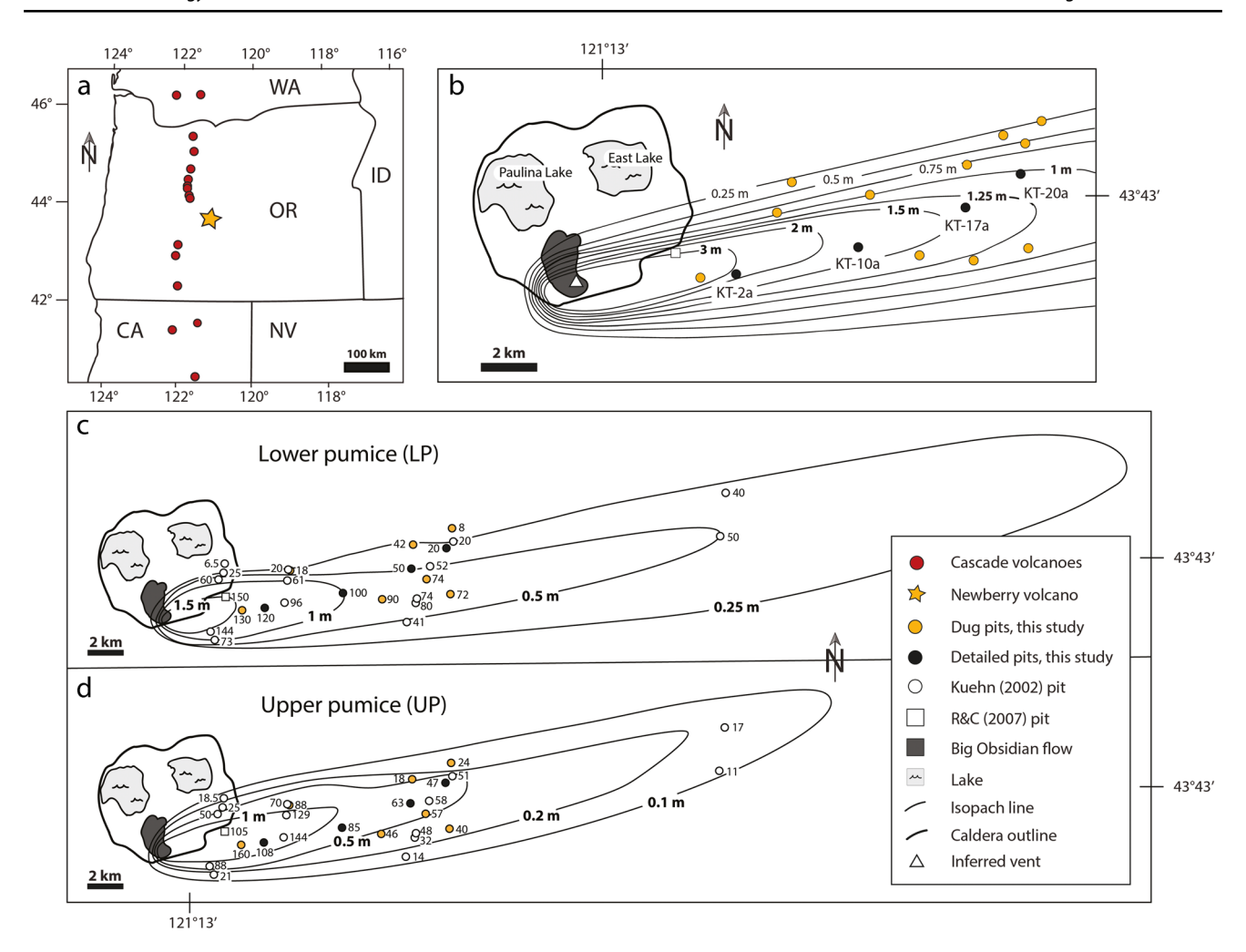


Fig. 1 a Locality map of Newberry Volcano, central OR, U.S.A. **b** Newberry Volcano, where black lines are isopach lines delineating entire deposit thickness for its 1300 BP eruption. R&C (2007) refers to Rust and Cashman's (2007) sample site, which is the same as Kuehn's (2002) 97–5 site. **c** Lower pumice deposit and **d** Upper pumice

deposit inferred by pit data from this study, Kuehn (2002), and Rust and Cashman (2007). Lower pumice's 0.25 m line was drawn with the assumption that the eastern part of the deposit was all lower pumice, thus following Kuehn (2002)'s whole deposit 0.25-m isopach line

erupted explosively over 50 times in the past 600,000 years (Donnelly-Nolan et al. 2011). The fallout from these explosive eruptions at Newberry has been found in 5 states across the western U.S.A. (Kuehn and Foit 2006). Scoria cones and mafic lava flows cover the flanks of the volcano and extend ~ 100 km from the caldera that formed during an explosive event ~ 80,000 years ago (Jensen et al. 2009).

The 640 CE Big Obsidian eruptive period

The most recent eruption of Newberry was the 640 CE Big Obsidian Flow eruptive event. It began explosively with a convective eruption column that deposited the Newberry Pumice deposit (0.1 km³ DRE; Rust and Cashman 2007). A small pyroclastic flow was emplaced following column collapse (Paulina

Lake Ash Flow; 0.002 km³ DRE; MacLeod and Sherrod, 1988). The final phase of the eruption was effusive with the extrusion of the Big Obsidian Flow (0.1 km³ DRE; Sherrod and MacLeod 1979). The focus of this study is the Newberry Pumice (NP) deposit. The NP deposit extends E-NE from the inferred vent in the southern tip of the Big Obsidian flow (Fig. 1b). The 0.25 m isopach of the whole NP deposit extends ~60 km from the caldera towards Brothers, OR (Kuehn 2002; MacLeod et al. 1995). It attains an estimated near-vent thickness of > 13 m where 1-m blocks can be found (Sherrod 1997).

The components of the NP deposit are juvenile pumice and obsidian pyroclasts, and lithics. Pumices lapilli are generally light gray but can be darker if rich in microlites. Obsidian pyroclasts appear as translucent to black dense chips. Lithics include red/brown/gray mafic scoriaceous and



dense clasts (Kuehn 2002; Rust and Cashman 2007; this study). In the field, the NP deposit is easily distinguished from the yellow-orange deposit of the underlying 5670 BCE climactic eruption of Mt. Mazama that created Crater Lake (giiwas in the Native language of the Klamath Tribe; Bacon 1983; Klug et al. 2002).

The NP deposit has been previously divided into two units, the Lower Pumice (LP) and the Upper Pumice (UP), separated by an ash horizon and distinguished by a change in obsidian textures (Rust and Cashman 2007) and/or marked change in clast size (Kuehn 2002). Both phases were deposited in roughly the same direction (northeast), but the UP is slightly more northerly, both consistent with a~SSW-NNE wind during the eruption (Fig. 1c-d; Kuehn 2002; this study). The LP also tends to be thicker and better sorted (Kuehn 2002).

Gardner et al. (1998) interpret the NP deposit to be from a single Plinian event, with discrete ash layers resulting from pyroclastic surges. More recent interpretations favor a two-phase Subplinian event (Kuehn 2002; Rust and Cashman 2007) with the ash layer separating LP and UP to represent a pause between two explosive phases during which the upper conduit filled with magma. Rust and Cashman (2007) also interpret UP ash layers to represent density currents shed from the plume.

The Paulina Lake ash flow was also emplaced after the NP deposit and is found in exposures on the south shore of Paulina Lake and the south caldera rim (Kuehn 2002). It is comprised of poorly sorted ash and pumiceous lapilli (MacLeod et al. 1995), exhibits bedding in the lower half of the deposit, and varies in thickness from 0.5 to 2 m (Kuehn 2002). The ~1.8-km-long Big Obsidian Flow, which constitutes the final phase of this eruption, is within the caldera and attains thicknesses > 20 m (Fig. 1b; Sherrod 1997). The Newberry Pumice, Paulina Lake ash flow, and the Big Obsidian Flow are all silicic (72.8% SiO₂; Macleod et al. 1995) and geochemically identical in terms of major element composition (Kuehn 2002), reinforcing the idea that they are all part of a single eruption.

Methodology

Fifteen pits were dug across the Newberry Pumice deposit, including 8 pits located roughly on the main dispersal axes of the LP and UP (Fig. 1b–d). At each location, the entire Newberry Pumice deposit was excavated and divided in subunits, which were then measured for thickness, described in detail, photographed, and sampled. Bulk samples of several hundred grams of tephra were taken from varying stratigraphic heights at each pit and stored in plastic sample bags. Samples from four pits located on the dispersal axis (totaling

37 samples; Fig. 2) were analyzed for componentry, grain size distribution by mass, and texture. We did not perform a total grain size distribution, but still report grain size distribution by mass for each pit. The material was deposited under consistent wind direction and plume height during eruptive pulses (Kuehn 2002), indicating that the grain size distribution likely largely reflects conduit processes. One pit is proximal (5.8 km from inferred vent), two are medial (10.4 km, 12.7 km), and one is medial-distal (16.8 km). For one pit (KT-10a, at 10.4 km), we also measured the density of > 500 lapilli from 5 layers spanning the entire Newberry Pumice stratigraphy.

The same sample preparation and analytical procedure were used for all the samples. First, each sample was manually sieved every phi from 3 to -5ϕ (0.125 to 32 mm), where $\phi = -\log_2(d)$ and d is the particle equivalent diameter in millimeters. Each sieve fraction was (1) placed in an ultrasonic bath for 5 min, (2) dried overnight at 100 °C to remove adsorbed water, and (3) weighed using a high-precision balance (precision: 10⁻⁴ g). For lapilli, fines adhering to the larger clast were discarded. Point count componentry was done on 100–450 clasts for every size fraction (every ϕ). Individual grains were counted and sorted as juvenile pumice, juvenile obsidian, or lithics (Fig. 3). Obsidian may appear as clear glass (Fig. 3c), but it is geochemically identical to black obsidian (Rust and Cashman 2007). Any larger size fractions wherein the number of clasts precluded a statistically robust analysis (i.e., number of clasts < 100) was noted.

For each sample, we evaluated the exterior texture of 50--100 clasts of 8--16--mm pumice lapilli $(-4 < \phi < -3)$ under a microscope. We noted whether each lapillus exhibited breadcrusting/fractures, banding of alternating obsidian-like and pumice-like textures, or evidence of sintering, wherein clasts appear to be amalgamations of smaller clasts, having juxtaposed texturally-distinct domains that can trap oxidized ash and/or lithic material (Trafton and Giachetti 2021; Giachetti et al. 2021; Fig. 3d, e). We also recorded whether the clast texture was predominantly tubular (i.e., largely comprised of elongated bubbles; Fig. 3f), or homogeneous (i.e., containing more spherical bubbles). Microphenocrysts/xenocrysts were also noted.

For pit KT-10a (Figs. 1 and 2), we measured the volume of > 100 lapilli per sample for five samples collected 15–40 cm apart vertically. These lapilli are all within the same ϕ (8–16 mm in diameter) per the suggested methodology (Houghton and Wilson 1989; Shea et al., 2010). Clast density was directly obtained using the classical immersion method (Houghton and Wilson 1989) or, for smaller clasts, calculated by dividing the mass of the clast obtained with a high-precision balance by its volume measured via a Microtrac PartAn 3D particle size analyzer (\pm 5–10%; supplementary methodology, Trafton and Giachetti 2021; Wiejaczka



Bulletin of Volcanology (2022) 84:104 Page 5 of 18 104

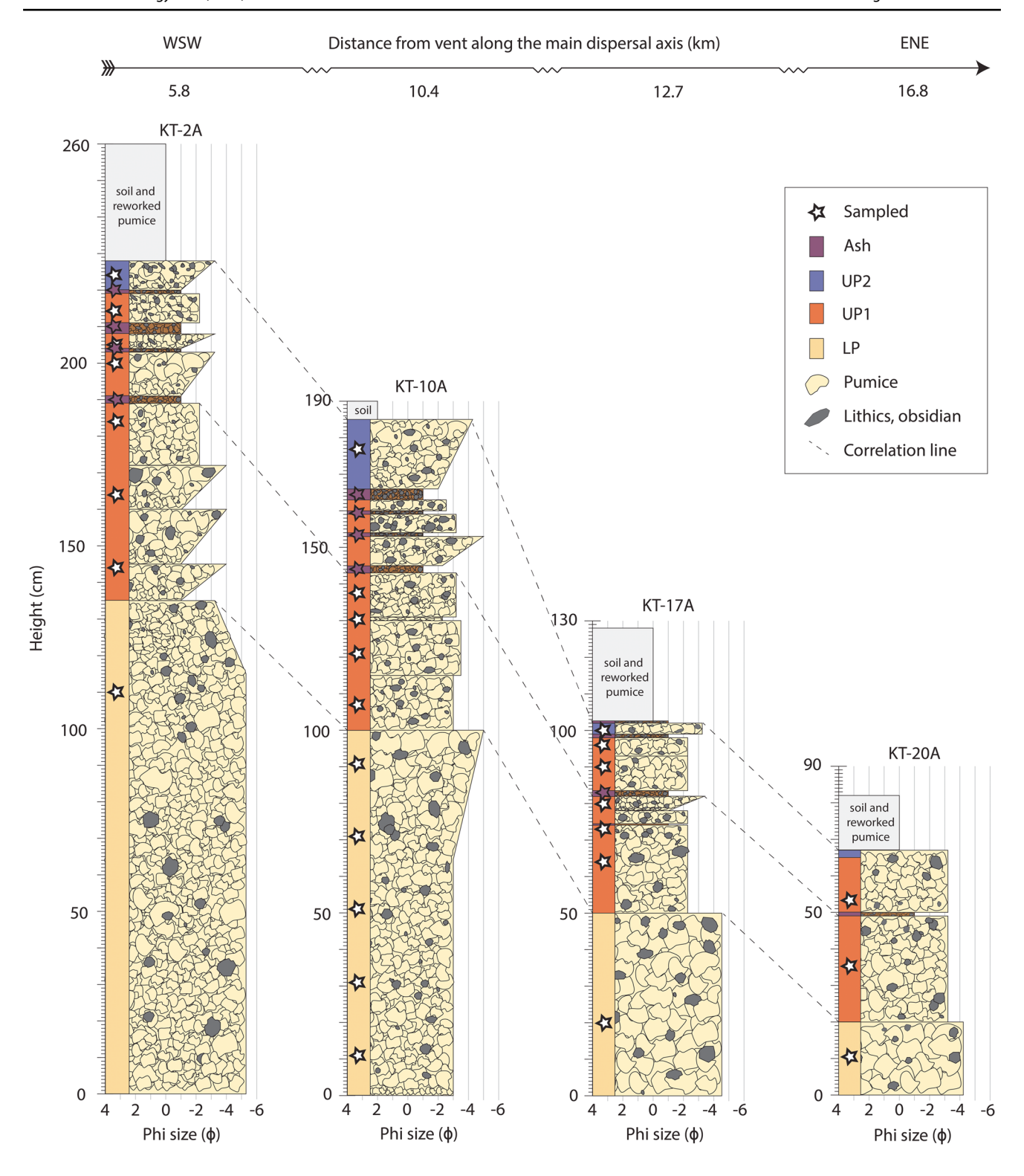


Fig. 2 Stratigraphic columns of the four sampled pits based on field observations. Depth is represented vertically wherein 0 cm is the contact between the Newberry and the underlying Crater Lake-giiwas deposits. Average clast size in the horizontal based on field observa-

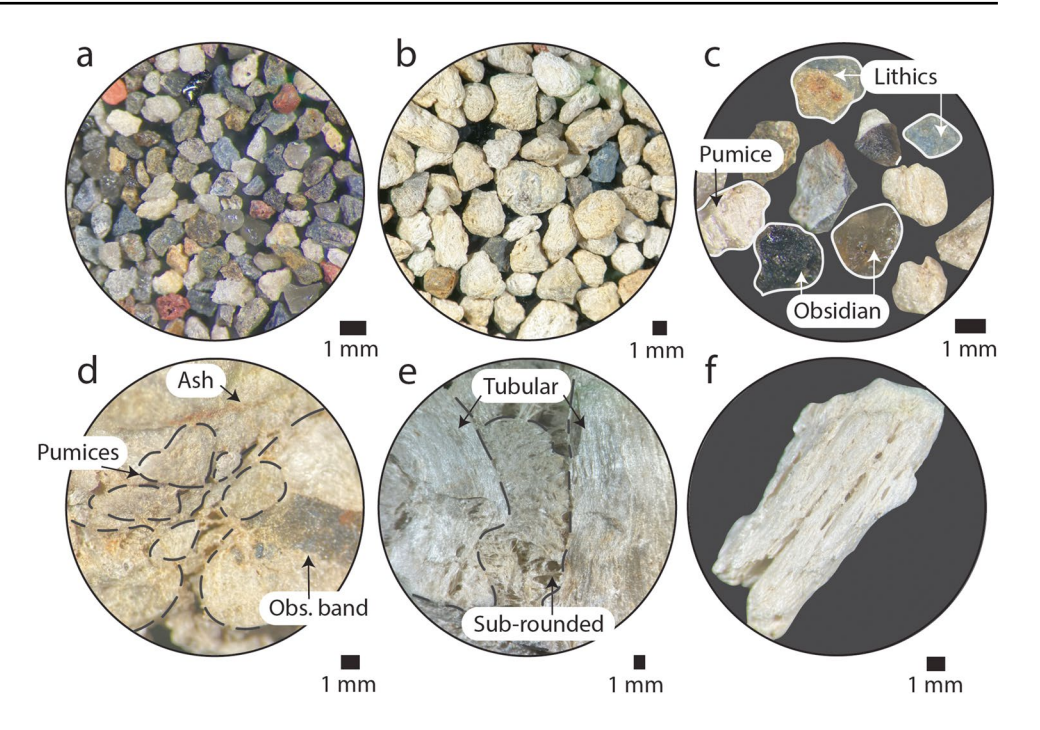
tions. Colored bars indicate classification of layers as Lower (LP), Upper (UP1), and Uppermost (UP2) Newberry pumice. Ash layers are also indicated in purple. Sampled layers are starred

and Giachetti 2022). We report and plot data in terms of both density (ρ) and porosity (α) , and similarly report size

in terms of diameter (*d*), volume (*V*), and phi size (ϕ). Clast porosity, α in %, is given by



Fig. 3 Physical attributes of samples. a Ash-sized (0.25- $0.5 \text{ mm}; -1 < \phi < -2) \text{ bulk}$ sample rich in lithics and obsidian. **b** Pumice-dominated lapilli sample (2–4 mm; $1 < \phi < 2$). **c** Components: pumice, obsidian, and lithics. d Sintered pumiceous clast made of amalgamated pumice, ash (red-brown line), and obsidian, e Another type of sintered clast wherein clasts with disparate bubble domains are juxtaposed (i.e., tubular and ~ spherical). f A tubular pumice—an elongated clast with elongated vesicles



$$\alpha = (100 \times M) / (\rho_s \times V) \tag{1}$$

where M is the mass of a particle, V is its volume, and $\rho_s = 2.32 \pm 0.01$ g cm⁻³ is the density of the solid phase (Giachetti et al. 2021).

We calculated the volume fraction of the three components (juvenile pumice, juvenile obsidian, lithic) in each of the 37 layers investigated, taking into account the relative volume of the eight size fractions, from 3 to -5ϕ . This volume fraction of the different components is the weighed sum of the componentry, where the weight is the relative volume represented by the size fraction. We used the relative mass of each size fraction (wt.%), the componentry of each size fraction (vol.%, considered equal to the point count), and the density of each of the three components (g cm⁻³). We assumed that obsidian pyroclasts of all sizes have the density of the bubble-free rhyolitic glass (2.32 g cm⁻³; Giachetti et al. 2021). Similarly, we used a constant density of 2.8 g cm⁻³ (typical density of basalt) for all lithics. For pumices, we used a log-linear relationship between size and density (Bonadonna and Phillips 2003; Trafton and Giachetti 2021), wherein particles smaller than 8 microns have a density of 2.32 g cm⁻³ (i.e., dense glass), a reasonable assumption as, based on scanning electron microscope images, few bubbles persist below 8 microns in lapilli. Particles larger than 8 mm have a density of 0.66 g cm⁻³, which is equal to the average density of the five hundred 8-16-mm lapilli analyzed for density.



At any given proximal or medial pit investigated, the LP comprises $\sim 60 \pm 5\%$ of the total Newberry Pumice deposit thickness, and presents as a relatively coarse, singular unit of pumiceous lapilli. At 2 km northeast of the vent, it is > 1.5 m thick and thins to 0.25 m by ~40 km away along the main dispersal axis. The UP is also largely pumiceous but exhibits alternating units dominated either by lapilli- or ash-sized particles (Fig. 2). At 2 km northeast from the vent, the UP can be > 1.5 m thick, but thins to 0.1 m at ~ 30 km from the vent along the main dispersal axis. We further divide UP into UP1 and UP2, wherein UP2 is the final lapilli-dominated layer and UP1 is stratified with alternating lapilli and ash layers. The division is made as UP1 is texturally distinct from UP2, containing obsidian with highly variable textures (i.e., with xenocrysts and/or juxtaposed domains of spherical versus elongate bubbles; Table 1; Rust and Cashman 2007). UP2 also has a higher amount of obsidian and lithics in general, an observation also made by Rust and Cashman (2007). We thus present results in terms of the "LP," "UP1," and "UP2" sections of the deposit. We also amalgamate data from all ash layers within UP1 given their similarity in componentry, color, and grain size distribution by mass (Fig. 4). Results are summarized in Table 1.

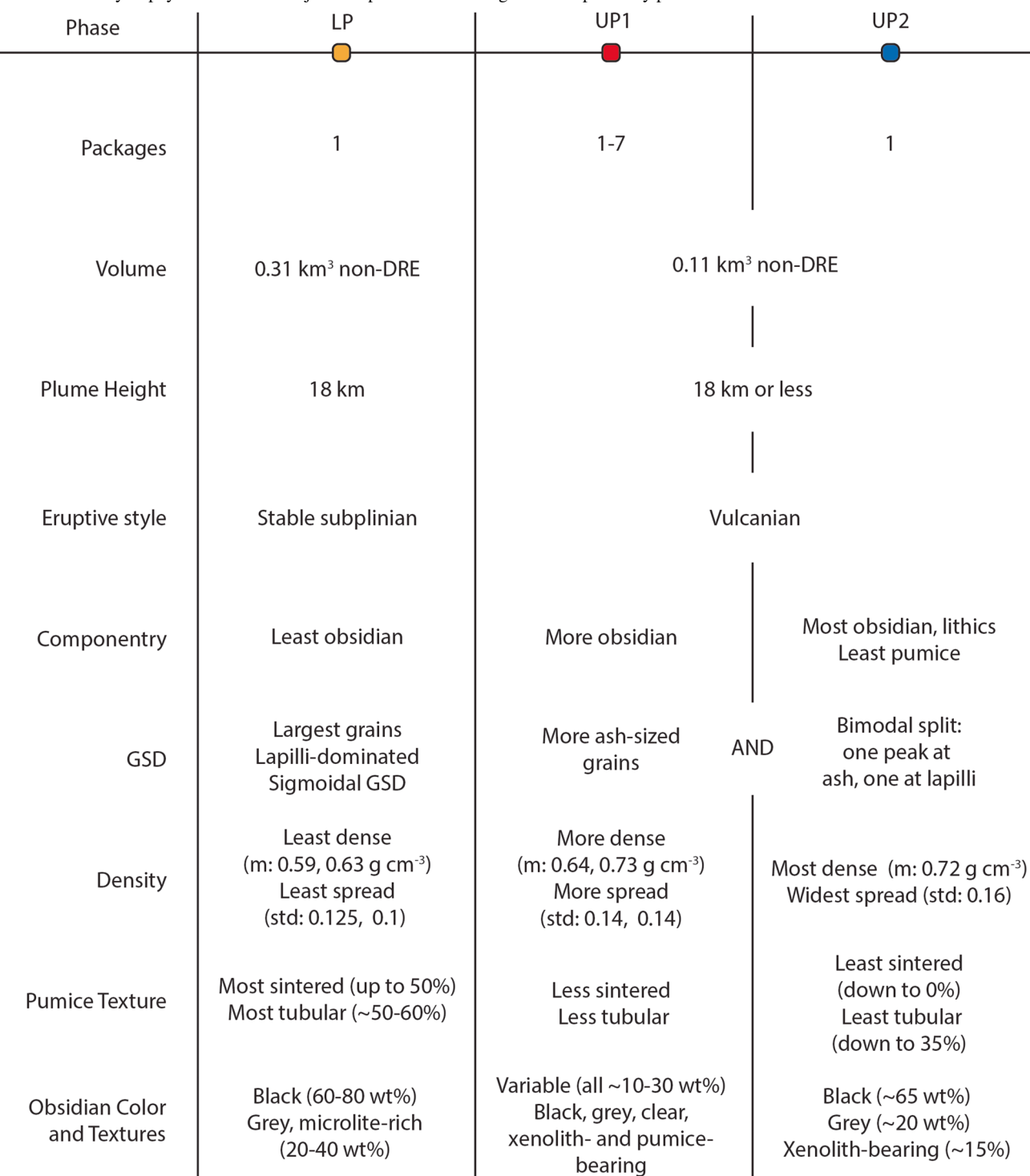
General trends

Regardless of section, pyroclast size is positively correlated with pumice content within each sample, from



Bulletin of Volcanology (2022) 84:104 Page 7 of 18 104

 Table 1
 Summary of physical attributes of juvenile products of the Big Obsidian period by phase



30–55% pumice at ~0.25 mm to 95–100% pumice for clasts larger than ~1 cm (Fig. 4). Conversely, size is inversely correlated with lithic and obsidian content. However, for the smallest size fraction analyzed (ϕ = 2–3), pumice content markedly increases while lithic content

decreases, potentially resulting from post-sampling abrasion. No obsidian clasts larger than 16 mm were found for any section from the pits surveyed; however, more proximal pits do have obsidian of this size (Rust and Cashman 2007; field observations during this study). Less than 1%



104 Page 8 of 18 Bulletin of Volcanology (2022) 84:104

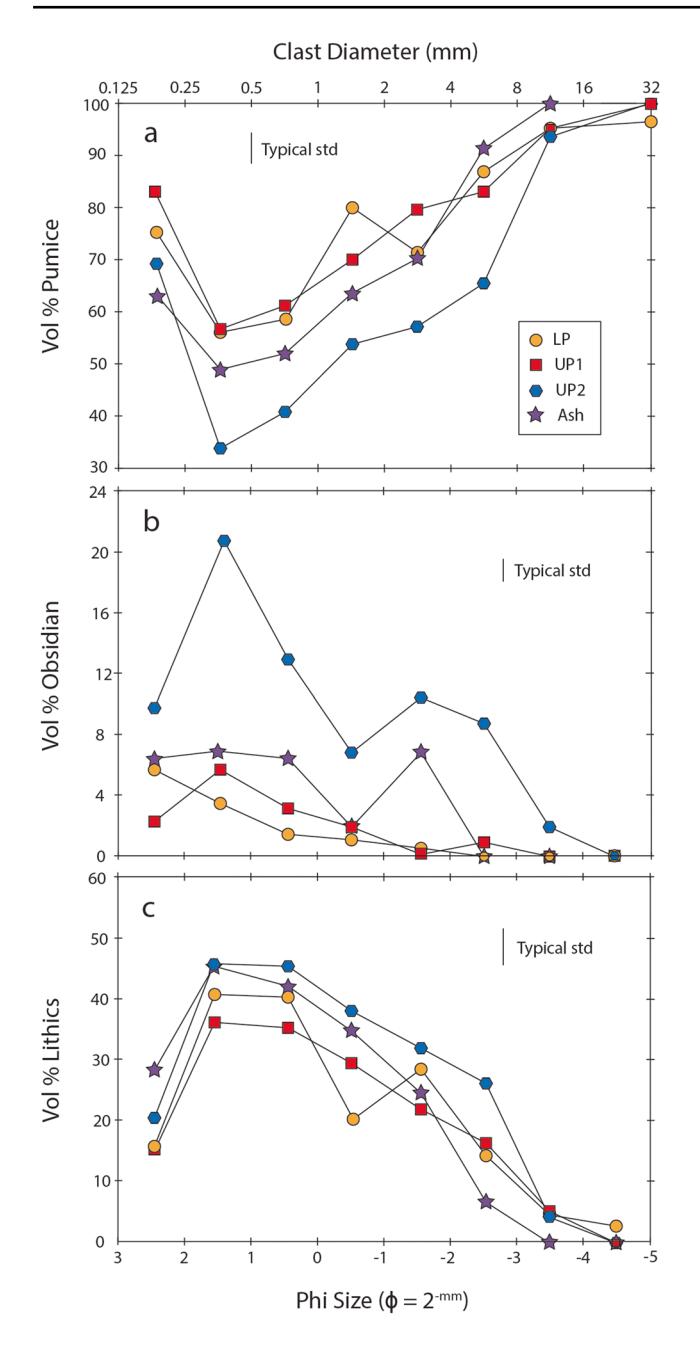
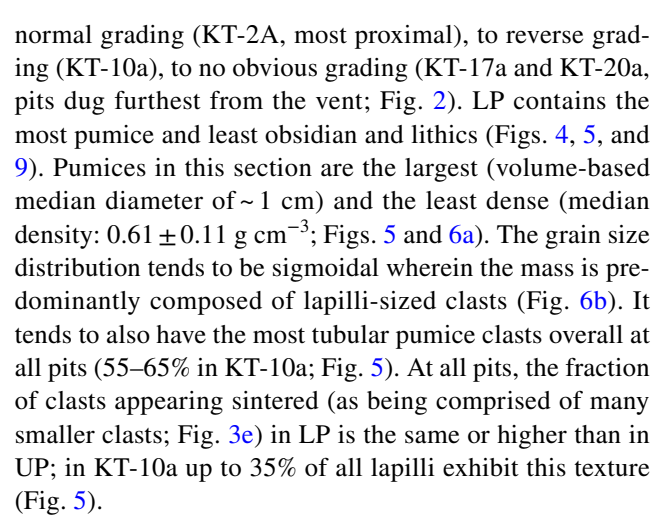


Fig. 4 Componentry of bulk samples sieved every phi and amalgamated stratigraphically as lower (LP), upper (UP1), uppermost (UP2), or ash for pit KT-10a. Here shown is clast size (in diameter and phi) versus **a** volume % pumice, **b** volume % obsidian, and **c** volume % lithics. Typical standard deviation given for LP, UP1, and ash; there is only one sample for UP2

of the > 3000 pumiceous clasts surveyed exhibited obsidian banding or breadcrusting. Less than 3% contain macroscopic crystals.

Lower Newbery Pumice (LP)

The lower deposit is one massive pumice-supported unit whose grading changes with distance from the vent from



Upper Newberry Pumice 1 (UP1)

Lapilli-dominated layers

The lapilli-dominated layers of UP1 are generally finergrained than those of LP (Figs. 5 and 6b). Proximal to medial deposits may exhibit several units of up to 10-cm-thick layers that are massive or reversely graded (Fig. 2). These layers contain a higher fraction of obsidian pyroclasts and lithics as compared to the LP (Fig. 5). The amount of tubular pumice varies at KT-10a (30–78%), but on average UP1 contains fewer tubular lapilli than compared to LP (Fig. 5). About 5–12% of lapilli clasts appear sintered at KT-10a. Pumiceous lapilli are also denser than in the LP (median density: $\sim 0.70 \pm 0.14$ g cm⁻³; Fig. 6a). The grain size distribution shifts to lower sizes and exhibits a bimodal distribution with one peak at $\phi \sim -2 \pm 0.5$ (~ 4 mm) and the other at $\phi \sim 0.5$ (~ 0.75 mm; Fig. 6b), with a volume-based median diameter around 4 mm (Fig. 5).

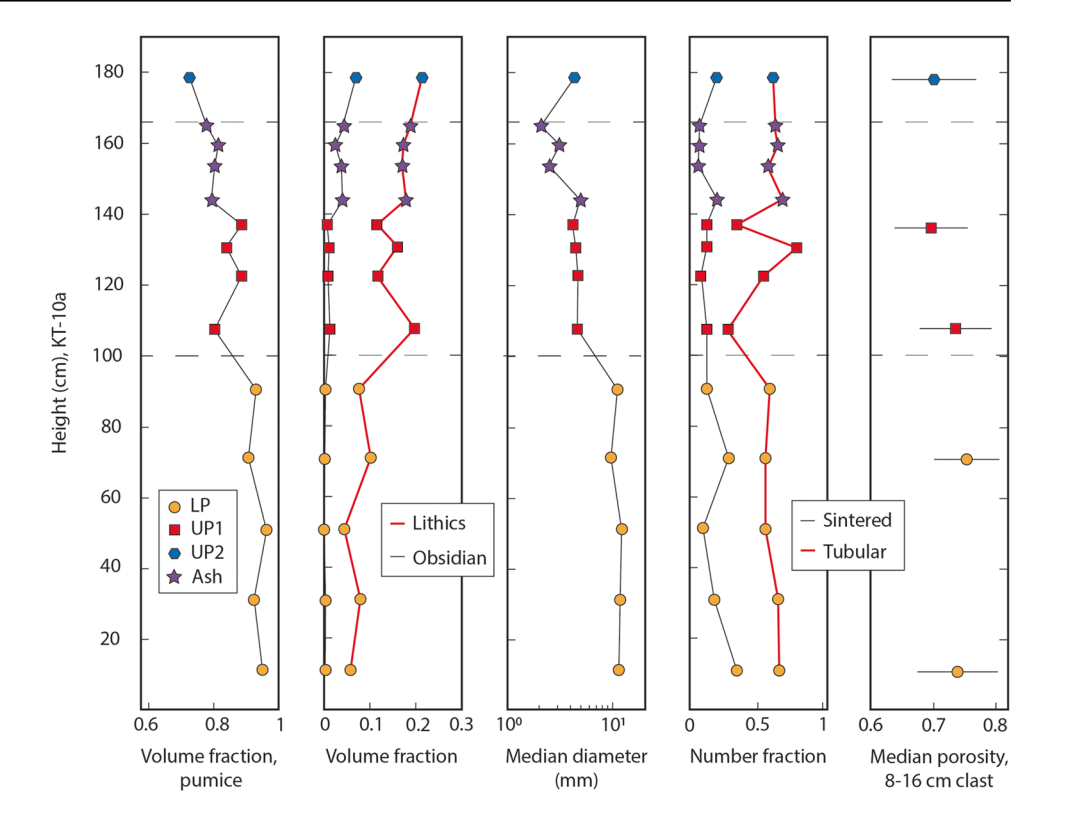
Ash-dominated layers

The ash layers that appear in the upper third of UP1 are a few centimeters thick at most (Fig. 2) and are flat-lying with a consistent thickness at each pit. They appear grey to mahogany brown in the field and tend to be riddled with roots, particularly just below UP2 (Fig. 2). The number and thickness of the ash layers vary from pit to pit from none to seven, as deposition of larger clasts in vent-proximal locations may have resulted in the destruction of delicate ash layers (Kuehn 2002). The first centimeter(s)-thick ash layer above the first few units of upper lapilli layers in UP1 is used as a datum to correlate three of the pits based on its componentry, color, and consistent thickness in proximal and medial pits (Fig. 2). The ash-dominated layers contain a much higher portion of obsidian pyroclast and a slightly higher proportion of lithics



Bulletin of Volcanology (2022) 84:104 Page 9 of 18 104

Fig. 5 Physical data by stratigraphic layer for pits KT-10a. Similar general trends are apparent in other pits. LP is Lower Pumice, UP is Upper Pumice



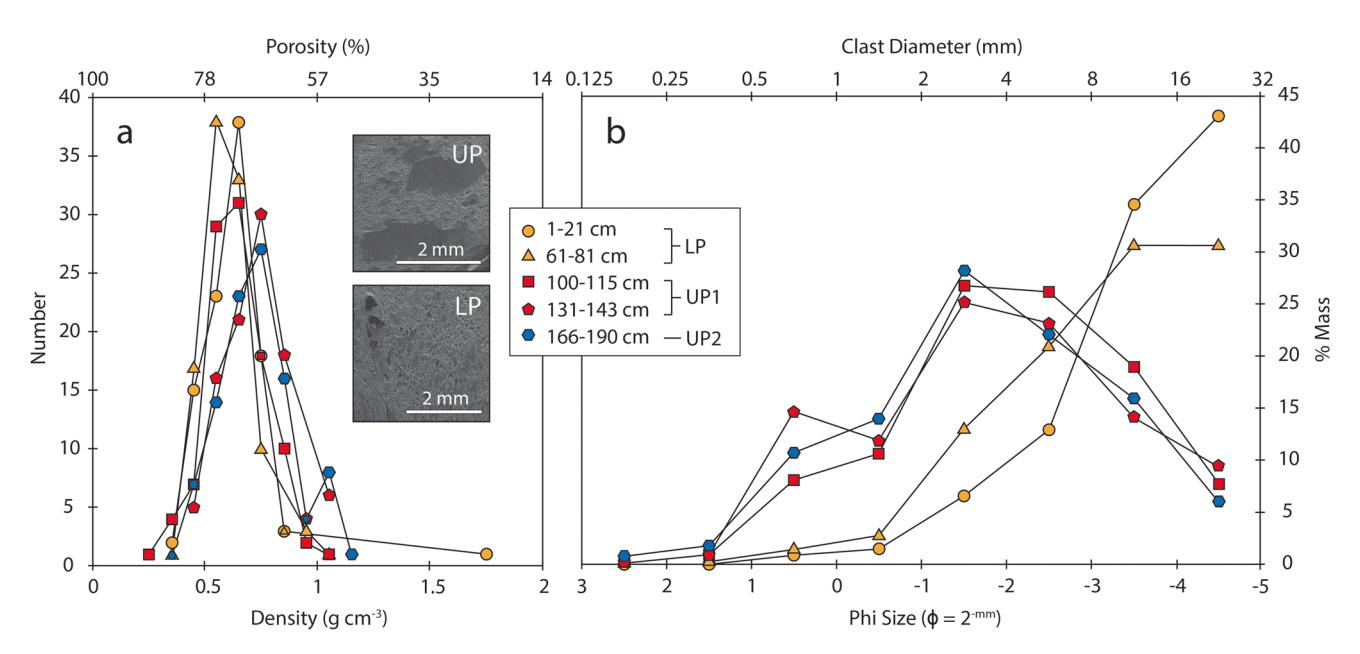


Fig. 6 a) Density and b) grain size distribution by mass for different layers from pit KT-10a. The legend is for both a) and b). SEM images are of internal and external texture of a typical pumiceous clast from the c) LP and d) UP

compared to their lapilli-dominated counterparts in UP1. At KT-10a, the proportion of tubular clasts per layer is 57–68%. Sintered lapilli comprise 6–21% of clasts, though three of the layers notably have only 6–7% of sintered clasts (Fig. 5).

Upper Newberry Pumice 2 (UP2)

The UP2 section is a lapilli-dominated layer that is slightly finer than most of the lapilli-dominated layers of UP1 (Fig. 5). This layer coarsens upwards in proximal and medial



104 Page 10 of 18 Bulletin of Volcanology (2022) 84:104

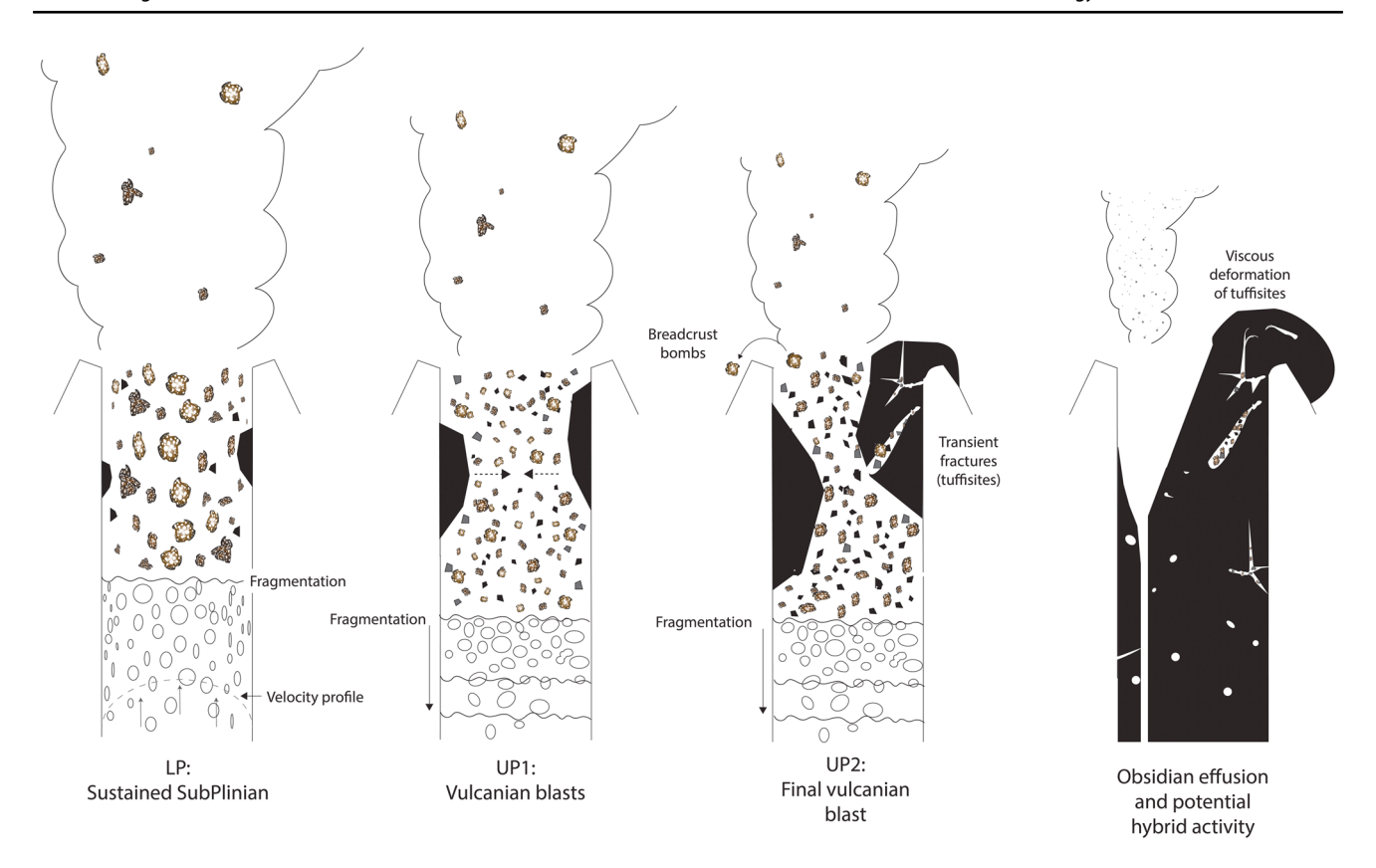


Fig. 7 Conduit model of the Subplinian eruption, which began with a sustained plume, transitioned to pulsatory explosions, and finished with lava effusion following concurrent explosive-effusive activity

pits (Fig. 2), a feature that is less evident as the distance from the vent increases. UP2 has more lithics and markedly

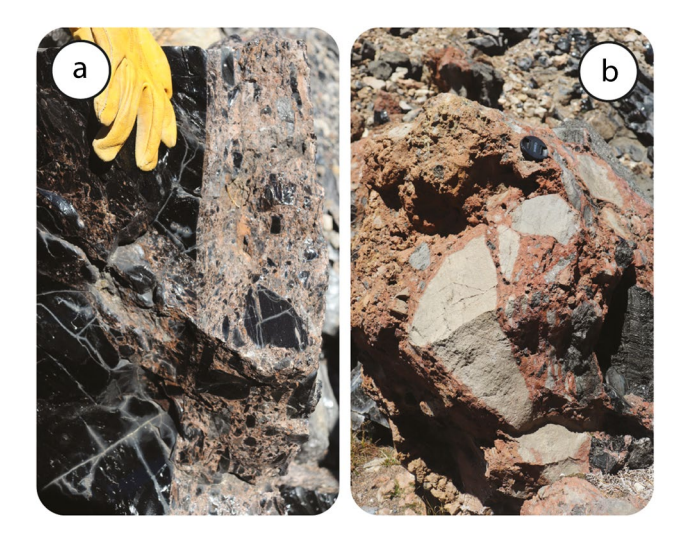
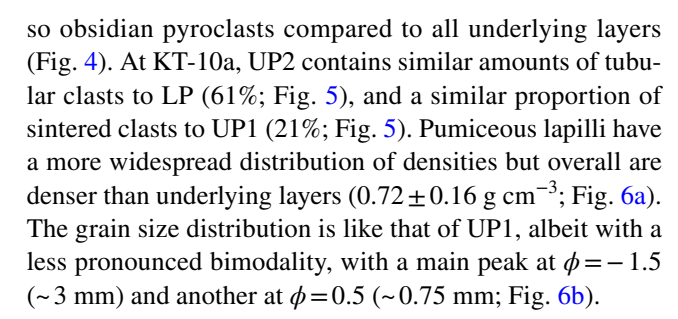


Fig. 8 Found on the Big Obsidian Flow < 1 km from the interpreted vent (Kuehn 2002), composite bombs (Schipper et al. 2021) include a flow tuffisite, in which the ash-filled veins choked with lithics and pumiceous clasts directly contacts dense, black glass, and b ballistic tuffisite, in which an ash matrix sinters together blocks (Tuffen et al. 2003; Castro et al. 2014). Camera lens cap for scale in b



Discussion

The continuity of the 640 CE eruption at Newberry

Below, we discuss our interpretation of the continuity of the 640 CE eruption of Newberry also summarized in Fig. 7. We keep our interpretation in terms of LP, UP1, and UP2. As wind conditions and likely column height were consistent during pulses (Kuehn 2002), stratigraphic units roughly correlate to eruptive phases. However, because sedimentation is still largely dependent on clast size and shape (Saxby et al. 2020), we evaluated lapilli textures and shape from throughout each eruptive layer, rather than pulling from singular cm-scale intervals within a layer.



LP

Based on deposit extent (Fig. 1), sorting, grading, and juvenile material's characteristics, we interpret the LP deposit to be from a sub-Plinian stable plume, consistent with the interpretation from Kuehn (2002) and Rust and Cashman (2007). The LP is well-sorted and predominantly pumice (Figs. 4, 5 and 6a), as would result from a steady plume. The layer is normally graded in near-vent deposits, likely from a decrease in mass discharge rate over time. This is consistent with a decrease in both the median particle diameter and the proportion of tubular pumices (Figs. 5 and 6b).

The predominance of tubular lapilli in LP (55–65% in KT-10a; Fig. 5) indicates higher ascent rates (Taddeucci and Wohletz 2001; Palladino et al. 2008). LP also has the greatest number of amalgamated and partially sintered clasts (9–35% in KT-10a; Fig. 5). Inter-clast collisions occurred while clasts could still viscously deform, a process that happens immediately after fragmentation in (sub-)Plinian eruptions wherein the timescale of sintering is on par with the ascent timescale (Gardner et al., 1996; Giachetti et al. 2021). This amalgamation is more likely to occur near conduit walls, where collision likelihood is higher (Dufek et al. 2012). Although clasts collided in the conduit, secondary fragmentation seems comparatively low as there is only one main peak in the particle size distribution (Fig. 6b). Limited secondary fragmentation could result from relatively shallow fragmentation (Dufek et al. 2012; Giachetti et al. 2021). Provided ascent rate remains constant during LP, shallow fragmentation allows more time between bubble nucleation and sample quench, which could also explain why LP pumice lapilli are more porous and preserve large bubbles than lapilli created later during the eruption (Fig. 6c, d; Gonnermann and Manga 2007).

While pumice lapilli record dynamics closer to the inner conduit (Trafton and Giachetti, 2021), obsidian pyroclasts from welded ash can capture conduit margin dynamics (Gardner et al. 2017; Watkins et al. 2017). The Newberry 640 CE Big Obsidian event is similar to the 1325–1350 CE North Mono Craters eruption in scale and eruptive style (Gardner et al. 2017; Sieh and Bursik 1986). Both eruptions preserve obsidian pyroclasts that in part derive from ash amalgamation and sintering along conduit margins (Gardner et al. 2017; Wadsworth et al. 2020) based on textural characteristics (Rust and Cashman 2007). The proportion of obsidian pyroclasts found in LP tephra is extremely limited (<0.3 vol.%; Fig. 5), especially compared to the later UP (up to 4 vol.%). They are also homogeneous in texture (Rust and Cashman 2007), and have a limited breadth of water content suggesting formation or equilibration at shallow levels (< 1 km depth; Rust and Cashman 2007).

UP1

Following a cessation in surface activity as marked by a ~ cm-thick ash layer, the eruption changed to be more pulsatory in nature during UP1 (Fig. 7). Often, reversely graded lapilli layers are interspersed with ash layers. Rust and Cashman (2007) interpret this phase to still represent sub-Plinian activity, though more unsteady. Given the following observations arising from our detailed textural and componentry work, we propose that the eruption was rather Vulcanian-like in nature, wherein the conduit was repeatedly sealed by a dense plug between explosive pulses, then reopened and partly emptied during the explosive event itself (Druitt et al. 2002; Wright et al. 2007).

First, Vulcanian eruptions are comparable to sub-Plinian eruptions in terms of dispersal area, but tend to contain more fine material (Walker 1973; Cas and Wright 1987), a characteristic evident when comparing UP1 to LP (Fig. 6). Second, pumice lapilli in UP1 have slightly lower median porosity (70-73%) compared to LP (74-75%; Fig. 5), also a characteristic of Vulcanian eruptions compared to Sub-Plinian ones (Mueller et al. 2011). These denser lapilli (Fig. 6a) could derive from conduit margin fallback of more-degassed magma (Kennedy et al. 2005) or the sampling of variably degassed magma during Vulcanian pulses just below a dense plug (Giachetti et al. 2010; Burgisser et al. 2010). Third, fewer tubular pumices on average are found in UP ($\sim 40\%$) compared to the LP (55–65%), which could result from a switch to a top-down style of eruption in which sudden depressurization of magma following plug rupture drives rapid volatile exsolution and fragmentation of deeper magma (i.e., Vulcanian style; e.g., Druitt et al. 2002; Wright et al. 2007; Giachetti et al. 2010). In such a configuration, the magma would have less time to be sheared prior to quench as compared to during continuous rapid ascent (i.e., sub-Plinian/Plinian eruption). Finally, the GSD shifts to a bimodal distribution during UP1 (Fig. 6b), which may be the result of enhanced secondary fragmentation in the conduit. During pulses, the initial opening of the conduit may have led to more particles incorporated into the eruption column, increasing the likelihood of collision (Fig. 7). A switch to Vulcanian style during which magma is fragmented at deeper depths would also increase secondary fragmentation, as frequency of disruptive inter-particle collisions increases with fragmentation depth (Dufek et al. 2012). A narrower conduit would also make particle collisions more likely.

The lapilli-dominated layers of UP1 contain more lithics (11–19 vol.% in KT-10a; Fig. 5) than do those in LP (4–10 wt%), and their ash-dominated counterparts contain even higher amounts of lithics (17–19 wt%). Each ash layer could derive from the explosion of a small plug formed by



the agglomeration and sintering of juvenile ash along the conduit sides (i.e., obsidian pyroclasts). Towards the end of LP, more ash could have aggregated than was removed as the mass discharge rate decreased, perhaps mirroring an overall decrease in the magma supply rate at the base of the conduit. Ash accumulation on the conduit sides may have narrowed and nearly clogged the conduit (Schipper et al. 2021), allowing pressure to build underneath. The conduit would thus be more unstable and prone to future oscillating eruptive events (Aravena et al. 2018). The resulting plug would be made of partly degassed rhyolite from ash agglomeration and sintering and lithic fragments (UP1; Figs. 2 and 8c; Wadsworth et al. 2020) that fell from unstable vent walls (cf., Fig. 16a of Adams et al. 2006), consistent with the observation that many obsidian pyroclasts from UP1 preserve xenoliths (Rust and Cashman 2007). Once sufficient pressure builds under this loose plug, it ruptures and a Vulcanian cycle starts.

UP₂

We interpret the UP2 section as one last Vulcanian event capturing the transition in eruption dynamics to the beginning of effusive behavior with the emission of the Big Obsidian Flow, a rhyolitic lava flow. We find breadcrust bombs < 2 km due east from the vent, common products of Vulcanian explosions (Wright et al. 2007; Giachetti et al. 2010). UP2 layers are often reversely graded (Fig. 2; Kuehn 2002; Rust and Cashman 2007), which could result from a narrowing conduit. As the conduit narrows, ascent velocity would increase, allowing larger clasts to be deposited in the same location.

Compared to UP1, the sharp increase in obsidian (~7 vol.% compared to <1 vol.% in UP1 at KT-10a) and increase in lithic content (>21 vol.% in UP2 compared to 11–19 vol.% in UP1) both capture a final explosion that excavated more wall material relative to magma compared to previous pulses (Fig. 5). Lapilli are also the most variably dense (Figs. 5 and 6a), perhaps resulting from magma fragmented over a wider range of conduit depths (Clarke et al. 2007; Giachetti et al. 2010; Burgisser et al. 2010). The bimodal GSD (Fig. 6b) suggests increased secondary fragmentation, likely in conduit as more wall material collided with juvenile material in a narrowing conduit.

As bubbly magma was fragmented during UP2, co-effusion of degassed lava may have begun (c.f., Fig. 2c-d in Wadsworth et al. 2020). In UP2, we observe a marked increase in obsidian content at all sizes (Figs. 4 and 5). According to Rust and Cashman (2007), these obsidian pyroclasts have also volatile contents consistent with shallow depth formation. The overall increase in obsidian, as well as the relative lack of xenocrystic material preserved in obsidian, suggests a marked build-up of

obsidian forming laterally farther from the margins of the conduit, towards its center. This obsidian is also singularly textured and black (Rust and Cashman 2007), evidence that it had more time to evolve texturally before excavation (Gardner et al. 2017). It is thus not unreasonable that UP2 occurred while the Big Obsidian Flow was starting to emplace. Consistent with this hypothesis, we find ballistically emplaced blocks with tuffisite veins < 1 km from the interpreted vent and flow tuffisite on the Big Obsidian Flow (Fig. 8; also reported by Kuehn 2002), which would have been ejected during UP2. Tuffisitic material preserves juxtaposed porous and dense veins, indicating degassing promoted through obsidian-plastered conduit margins. Such tuffisites have been cited as necessary for hybrid explosiveeffusive behavior (Castro et al. 2012, 2014; Black et al. 2016; Schipper et al. 2021).

Volume estimates of the conduit and Vulcanian plugs

LP produced a total of $0.31 + / -0.06 \text{ km}^3$ of deposit, indicative of a sub-Plinian-sized eruption (Cioni et al. 2015). This volume was calculated by fitting the isopach data derived from the thickness measurements of LP from Kuehn (2002), Rust and Cashman (2007), and this study (Fig. 1) using a Weibull function (Bonadonna and Costa 2013; Fig. 10). We applied a 10% uncertainty to both the thickness and isoline area measurements as is typically associated with isopach construction (e.g., Le Pennec et al. 2012; Engwell et al. 2013; Klawonn et al. 2014a, b). Assuming a packing fraction of 0.7 for the polydisperse tephra in the deposit (Kansal et al. 2002), $\sim 2.17 \times 10^8$ m³ of material was ejected during LP. Using the volume proportions of lithics (2.1–9.9 vol.%), juvenile obsidian pyroclast (0.1–0.3 vol. %), and juvenile porous material (90.0–97.9 vol. %) measured at the four locations along the main dispersal axis (cf.; Figs. 5 and 9), lithics and obsidian pyroclast account for an average of 4.85 vol.% $(1.05 \times 10^7 \text{ m}^3)$ and 0.06 vol.% $(1.2 \times 10^5 \text{ m}^3)$ of LP tephra, respectively. Heath et al. (2015) estimate the top of the magma chamber beneath the caldera at Newberry to be located 3 km below the surface based on tomographic imaging. If the 1.05×10^7 m³ of ejected lithics during LP come only from the carving of a new, cylindrical conduit of constant radius from the top of the magma chamber to the surface, the conduit had a diameter of ~ 67 m.

We presume that the 1.2×10^5 m³ of obsidian pyroclast found in the tephra of LP come from the post-fragmentation agglomeration, sintering, and erosion and ejection of ashsize particles along the conduit wall during LP (Gardner et al. 2017; Wadsworth et al. 2020). Had fragmentation occurred at ~ 1 km depth (Rust and Cashman 2007), the



Bulletin of Volcanology (2022) 84:104 Page 13 of 18 104

total volume of obsidian pyroclast excavated from conduit walls would equal ~57 cm in thickness. Given the ubiquity of obsidian throughout the LP deposit, the upper conduit would likely have been lined by several mm to a few cm of ash at any given moment for this quantity of material to be excavated over the course of LP.

Vulcanian activity during UP1 and UP2 led to the emplacement of $\sim 0.11 + / -0.02 \text{ km}^3$ (non-DRE) of tephra deposit or $\sim 1.5 \times 10^7$ m³ of fallout deposit per pulse on average assuming seven pulses as identified at KT-10a. This corresponds to approximately 1×10^7 m³ of particles assuming a packing fraction of 0.7 for the polydisperse tephra in the deposit. Because the thickness ratio of lapilli-dominated layers to ash-dominated layers is roughly 9:1 at KT-2a and KT-10a, we assume the componentry of the whole volume of tephra ejected by each Vulcanian event to be 90% like that of the lapilli-dominated layers (1.4 vol.% obsidian, 11.5 vol.% lithic) and 10% like that of the ash-dominated layers of UP1 (4.5 vol.% obsidian, 20.3 vol.% lithic). Thus, each Vulcanian event ejected an average of 0.14×10^6 m³ of obsidian pyroclast and 2.03×10^6 m³ of lithics. Using these numbers, the plug was at least 40 m thick if we assume that (1) it was made of dense obsidian that wholly sealed the 67-m-wide conduit and (2) it was entirely destroyed during the first Vulcanian event of UP1. Such a plug would be thicker if slightly porous. Lithics ejected during each UP1 Vulcanian episode likely derive from both pre-eruptive fallback of unstable vent walls and syn-eruptive erosion of the conduit. Phase UP2, the last explosive event before the ultimate switch to an effusive-dominant eruption, produced an even higher amount of lithics and obsidian pyroclast. Such a high concentration of components suggests an irremediable change to the geometry and size of the shallowest part of the conduit/vent. These physical changes could have forced the change to effusive-dominant behavior, though this does not preclude other forcings—such as a decrease in overpressure from the magma chamber—to have contributed (Cassidy et al. 2018).

Comparison with the 2011–2012 eruption of Cordón Caulle

The eruption of Cordón Caulle in 2011–2012 began with a Plinian phase that erupted rhyolitic tephra ~ 14 km into the atmosphere for ~ 30 h (Collini et al. 2013). The plume then fluctuated between 3–10 km high for the next 7–9 days (Collini et al. 2013). Vulcanian blasts began on day 4 of the eruption and continued with kilometers-high tephra until day 10 (Schipper et al. 2013; Pistolesi et al. 2015). On day 9, ballistic intensity spiked, after which hybrid explosive-effusive activity started. Lava emerged from the same vent that produced tephra, about 10 days after the onset of the first Plinian

explosion (Castro et al. 2012, 2013; Silva Parejas et al. 2012). Ash emission and lava effusion continued for several months before the eruption stopped (Pistolesi et al. 2015). The 640 CE eruption of Newberry began with a similar intensity (initial plume height of ~21 km then decreasing to ~18 km; Gardner et al. 1998) and likely progressed from sustained to pulsatory to hybrid activity as based on parallels in deposit characteristics.

The deposits of the 2011–2012 eruption of Cordón Caulle contain cm- to tens-of-cm thick whiteish lapilli-bearing layers (Units I and II), overlain by thinner, cm-scale, darker ash beds (Unit III) in the latter 20–30% of the stratigraphy of near-vent deposits (Pistolesi et al. 2015), with ballistic material in the most proximal deposits. Heterogeneous clasts (as seen in banded pumice and crystals at Cordón Caulle) and obsidian increase in the latter half of the eruption, as does the density of lapilli. We observe the same overall deposit characteristics and trends in the Newberry Pumice (Table 8). Both eruptions' pumiceous products also show similar textures, particularly in lower layers (LP, Newberry Pumice, Fig. 3, 7; layers A-F at Cordón Caulle, Figs. 13, 15, Pistolesi et al. 2015) wherein they exhibit a variety of vesicular network shapes (from rounded to complex, irregular vesicles).

Both eruptions' changes in bed thickness and grain size evidence a shift from a strong plume to a weakening and increasingly fluctuating phase. Pistolesi et al. (2015) attribute the range of juvenile clast textures (i.e., clasts with crystals and/or obsidian banding) to the existence of a fissure system feeding the eruption, wherein degassed denser magma accumulates in the narrower portions of the conduit during slower ascent. Such textural variability has been found in eruptions that are dike-fed and is often ascribed to lateral or vertical variability in the conduit (e.g., 1060 CE Glass Mountain eruption of Medicine Lake; Fink and Pollard 1983; 5750 BCE eruption of Mt. Mazama; Wearn 2002; Giachetti et al. 2021; 2008 eruption of Chaitén; Wicks et al. 2011). At Newberry, which was also likely dike-fed (Rust and Cashman 2007), we ascribe heterogeneities to lateral variations, and the change of heterogeneities with time to capture conduit shape evolution. At Cordón Caulle, pumice from lower stratigraphic layers has variable vesicle textures interpreted to be from strain localization during rapid ascent. While strain localization likely also played a part at Newberry, we note that complex vesicle textures could also be due to amalgamation and sintering of pyroclasts (Giachetti et al. 2021)—a mechanism also possible at Cordón Caulle given that such textures have been found regardless of conduit system (Fig. 15 of Pistolesi et al. 2015).

The onset of effusive behavior at Cordón Caulle has been interpreted to result from a decrease in mass discharge rate (Pistolesi et al. 2015) and, more recently, by the sintering of recently fragmented juvenile material (Wadsworth et al.



2020; Schipper et al. 2021). Schipper et al. (2021) investigated the textures of composite bombs (bombs composed of ash and tuffisitic material) produced during the change from pure explosive to hybrid activity at Cordón Caulle. These bombs preserve ash-dominated matrices and components of finely-fragmented material (Wadsworth et al. 2020), as well as fragmented partially sintered dense material, evidence of prolonged high-energy fragmentation (Spieler et al. 2004; Wadsworth et al. 2020). This sustained efficient fragmentation and sintering lead to ash agglomeration and subsequent lava effusion (Schipper et al. 2021), and these composite bombs thus show that explosivity can be self-extinguishing. The onset of effusive behavior was also supported by notable pervasive fracturing in the dike system and lava flow itself through tuffisite outgassing (Castro et al. 2014), aided by vein connection with exsolved gas in porous domains (Saubin et al. 2016).

At Newberry, we could envision a similar self-extinguishing eruptive behavior driven by efficient fragmentation and supported by tuffisitic outgassing. Obsidian pyroclasts and pumiceous products preserve juxtaposed textural domains (Rust and Cashman 2007), evidence of repeated fragmentation cycles in the conduit. The ejection of ash at the end of the explosive phase, like that at Cordón Caulle, may similarly result from earlier efficiently-fragmented material that could have also agglomerated into lava (i.e., forming the Big Obsidian Flow). Volatile contents in the UP2 do preserve a very shallow depth assembly/equilibration of products, as shallow as 0.2 km below the surface (Rust and Cashman 2007). Obsidian pyroclasts from similar eruptions also preserve very low (< 0.3 wt%; 2011 eruption of Cordón Caulle; Schipper et al. 2013; Castro et al. 2014) to low water content (< 1.6 wt%; 2008 eruption of Chaitén; Castro et al. 2014; Forte and Castro 2019) consistent with upper conduit formation of obsidian. Additionally, we do find evidence for tuffisitic ash venting in bombs on the surface of the Big Obsidian Flow (Fig. 8), which at other eruptions has been observed to accompany hybrid activity (Chaiten, Cordón Caulle; Schipper et al. 2013; Castro et al. 2014) or was interpreted as such via field observations (Mono-Inyo, USA; Black et al. 2016; Medicine Lake, USA; Castro and Walter 2021). Efficient outgassing was also likely enabled by conduit enlargement in the final phase, consistent with the high concentration of lithics and obsidian pyroclast in UP2.

Based on the similitude between the two eruptions, we thus estimate that the predominantly explosive phase of the 640 CE eruption of Newberry Volcano (LP, UP1, and UP2) lasted several tens of hours to several days at a maximum, compared to Cordón Caulle's climactic phase (Units I–III), which was ~ 12 days long. We tentatively suggest the predominantly effusive phase to be on the order of days to weeks (as opposed to several months at Cordón Caulle),

given the comparative smaller volume of the deposit to the effusive phase at Cordón Caulle (Newberry: ~0.1 km³ DRE, Cordón Caulle: 0.6 km³; Coppola et al. 2017). We additionally note that Pistolesi et al. (2015) also report locally preserved fallout layers of fine ash deposited during hybrid activity (Unit IV) that, about 10 years after the eruption, have been partly eroded and only found in the area close to the vent (H. Tuffen, J. Wiejaczka, personal communication). While fine, proximal ash layers may have been deposited during a hybrid explosive/effusive phase at Newberry (Kuehn 2002), we did not find such layers where we sampled. If indeed initially present in proximal areas, such layers of fine ash must have been completely eroded during the past ~ 1000 years since the eruption. Thus, the fallout deposit examined herein probably only capture the first ten(s) of days of the eruption as represented by Units I-III at Cordón Caulle (Pistolesi et al. 2015).

Conclusion

Based on sedimentological characteristics and physical aspects of juvenile products, we interpret the explosive phase of Newberry Volcano's 640 CE explosive phase to have transitioned from a relatively-stable sub-Plinian phase to Vulcanian-like pulses. The last Vulcanian event probably occurred at the same time as the onset of the final effusion of the Big Obsidian Flow. The seemingly progression of the eruption based on the tephra deposit is like that of the only two witnessed eruptions of crystal-poor rhyolitic magma at Chaîten and Cordón Caulle (Chile; 2008 and 2011–2012, respectively), suggesting a commonality in eruption progression for silicic crystal-poor eruptions. Additionally, all three eruptions have products containing tuffisitic veins, which are key to permitting outgassing and subsequent hybrid behavior (Stasusik et al. 1996; Castro et al. 2014; Black et al. 2016; Saubin et al. 2016; Wadsworth et al. 2020). When interpreted through the lens of recent advanced in conduit studies (Saubin et al. 2016; Gardner et al. 2017; Cassidy et al. 2018 and references therein; Wadsworth et al. 2020; Schipper et al. 2021; Ohashi et al. 2021; Castro and Walter 2021), these new data, together with previous work on the same eruption (Gardner et al. 1998; Kuehn 2002; Rust and Cashman 2007), support the interpretation that the 640 CE eruption of Newberry Volcano—particularly in the latter half of the eruption—was modulated by cycles of ash agglomeration, sintering, and excavation along conduit margins. Co-explosive-effusive behavior may be more prevalent than previously thought. Additionally, its record may only be evident by examining dense and porous endmembers of juvenile tephra in near-vent areas.



Bulletin of Volcanology (2022) 84:104 Page 15 of 18 104

Appendix

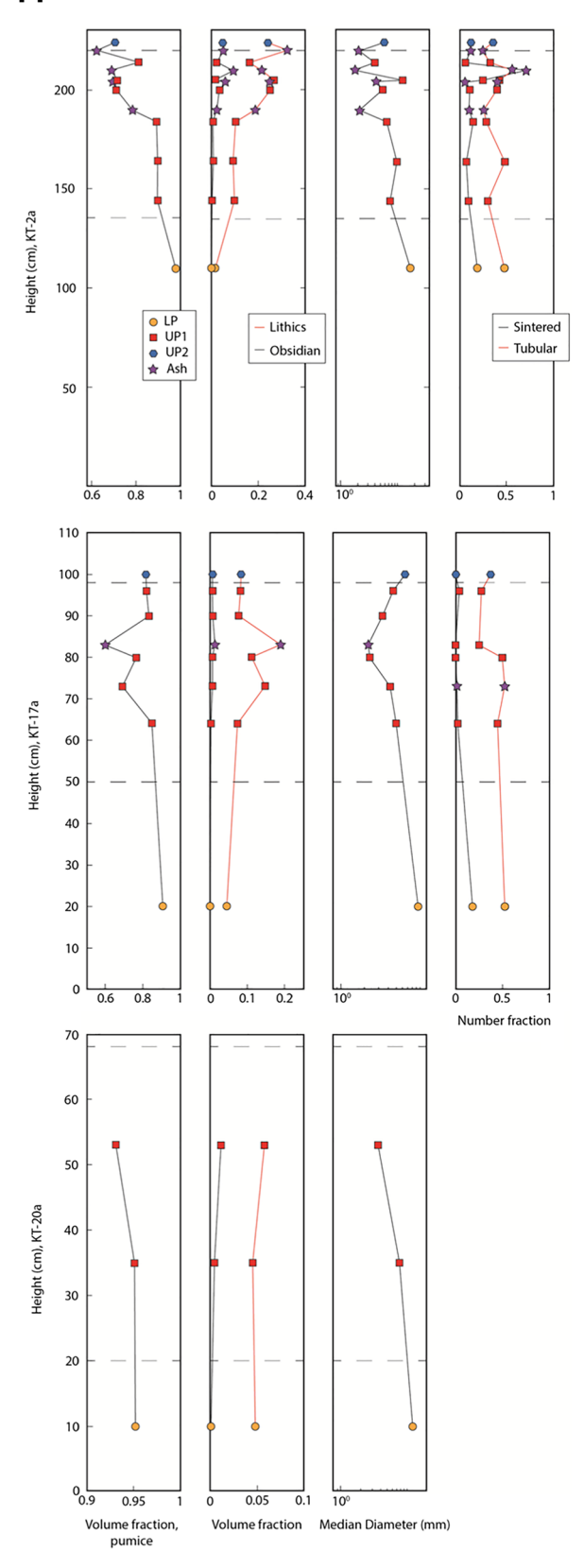


Fig. 9 Physical data by stratigraphic layer for pits KT-2a, KT-17a, and KT-20a. LP is Lower Pumice, UP is Upper Pumice

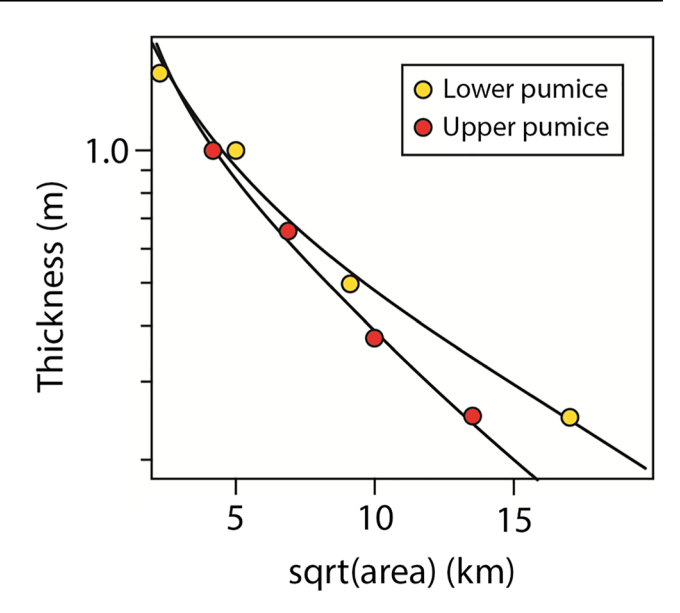


Fig. 10 Thickness of the Newberry a) Lower Pumice and b) Upper pumice versus the square root of the area of the corresponding isopach ellipse. Figure modified from an AshCalc model that fit the data using a Weibull function (Daggitt et al. 2014)

Acknowledgements Thank you to J. Wiejaczka for the help in the field and to the U.S. Forest Service for permitting us to dig and collect samples. We also thank N.B. Plumb who helped organize, sort, and classify some of the pumices. We thank Hugh Tuffen and an anonymous reviewer for their insight that greatly improved the manuscript. We also thank Ulrich Küppers and Jacopo Taddeucci for their care in editing and handling the manuscript.

Funding K.R. Trafton was partly funded by a grant from Sigma Xi and the Geological Society of America. T. Giachetti and K.R. Trafton were partly funded by the National Science Foundation grant EAR-1725207.

References

Adams NK, Houghton BF, Hildreth W (2006) Abrupt transitions during sustained explosive eruptions: examples from the 1912 eruption of Novarupta. Alaska Bull Volcanol 69(2):189–206

Alidibirov M, Dingwell DB (1996) Magma fragmentation by rapid decompression. Nature 380:146–149

Aravena Á, Cioni R, Vitturi MDM, Neri A (2018) Conduit stability effects on intensity and steadiness of explosive eruptions. Sci Rep 8(1):1–9

Austin-Erickson A, Büttner R, Dellino P, Ort MH, Zimanowski B (2008) Phreatomagmatic explosions of rhyolitic magma: experimental and field evidence. J Geophys Res Solid Earth 113(B11)

Bacon CR (1983) Eruptive history of Mount Mazama and Crater Lake caldera, Cascade Range, USA. J Volcanol Geoth Res 18(1-4):57-115

Baxter PJ, Horwell CJ (2015) Impacts of eruptions on human health. The encyclopedia of volcanoes: 2nd edition. Elsevier. pp. 1035–1047



104 Page 16 of 18 Bulletin of Volcanology (2022) 84:104

- Black AB, Manga M, Andrews B (2016) Ash production and dispersal from sustained Mono-Inyo eruptions. Bull Volcanol 78(57). https://doi.org/10.1007/s00445-016-1053-0
- Bonadonna C, Costa A (2013) Plume height, volume, and classification of explosive volcanic eruptions based on the Weibull function. Bull Volcanol 75(8):1–19
- Bonadonna C, Phillips JC (2003) Sedimentation from strong volcanic plumes. J Geophys Res Solid Earth 108(B7):1–28. https://doi.org/10.1029/2002jb002034
- Burgisser A, Arbaret L, Druitt TH, Giachetti T (2010) Pre-explosive conduit conditions of the 1997 Vulcanian explosions at Soufrière Hills Volcano, Montserrat: II. Overpressure and depth distributions. J Volcanol Geotherm Res 199(3–4):193–205
- Carey SN, Sigurdsson H (1982) Influence of particle aggregation on deposition of distal tephra from the May 18, 1980, eruption of Mount St. Helens volcano. J Geophys Res Solid Earth 87(B8):7061–7072
- Cas RAF, Wright JV (1987) Volcanic successions: modern and ancient. Allen Unwin London. https://doi.org/10.1007/978-94-009-3167-1
- Cassidy M, Cole PD, Hicks KE, Varley NR, Peters N, Lerner AH (2015) Rapid and slow: varying magma ascent rates as a mechanism for Vulcanian explosions. Earth Planet Sci Lett 420:73–84
- Cassidy M, Manga M, Cashman K, Bachmann O (2018) Controls on explosive-effusive volcanic eruption styles. Nat Commun 9(1):1–16
- Castro JM, Dingwell DB (2009) Rapid ascent of rhyolitic magma at Chaitén volcano, Chile. Nature 461(7265):780–783
- Castro JM, Gardner JE (2008) Did magma ascent rate control the explosive-effusive transition at the Inyo volcanic chain, California? Geology 36(4):279–282
- Castro JM, Walter SC (2021) Hybrid rhyolitic eruptions at Big Glass Mountain, CA, USA. Volcanica 4(2):257–277. https://doi.org/10.30909/vol.04.02.257277
- Castro JM, Cordonnier B, Tuffen H, Tobin MJ, Puskar L, Martin MC, Bechtel HA (2012) The role of melt-fracture degassing in defusing explosive rhyolite eruptions at volcán Chaitén. Earth Planet Sci Lett 333:63–69
- Castro JM, Schipper CI, Mueller SP, Militzer AS, Amigo A, Parejas CS, Jacob D (2013) Storage and eruption of near-liquidus rhyolite magma at Condon Caulle, Chile. Bull Volcanol 75:702
- Castro JM, Bindeman IN, Tuffen H, Schipper CI (2014) Explosive origin of silicic lava: Textural and δD–H2O evidence for pyroclastic degassing during rhyolite effusion. Earth Planet Sci Lett 405:52–61
- Cioni R, Pistolesi M, Rosi M (2015) Plinian and Subplinian eruptions. The encyclopedia of volcanoes: 2nd edition. Elsevier. pp. 519–535
- Clarke AB, Stephens S, Teasdale R, Sparks RSJ, Diller K (2007) Petrologic constraints on the decompression history of magma prior to Vulcanian explosions at the Soufrière Hills volcano, Montserrat. J Volcanol Geoth Res 161(4):261–274
- Clarke AB, Ongaro TE, Belousov A (2015) Vulcanian eruptions. The encyclopedia of volcanoes: 2nd edition. Elsevier. pp. 505–518
- Collini E, Osores MS, Folch A, Viramonte JG, Villarosa G, Salmuni G (2013) Volcanic ash forecast during the June 2011 Cordón Caulle eruption. Nat Hazards 66(2):389–412
- Coppola D, Laiolo M, Franchi A, Massimetti F, Cigolini C, Lara LE (2017) Measuring effusion rates of obsidian lava flows by means of satellite thermal data. J Volcanol Geoth Res 347:82–90
- Daggitt ML, Mather TA, Pyle DM, Page S (2014) AshCalc a new tool for the comparison of the exponential, power-law and Weibull models of tephra deposition. J Appl Volcanol 3:7
- Davies BV, Brown RJ, Barclay J et al (2021) Rapid eruptive transitions from low to high intensity explosions and effusive activity: insights from textural analysis of a small-volume trachytic eruption, Ascension Island, South Atlantic. Bull Volcanol 83(58). https://doi.org/10.1007/s00445-021-01480-1

- Di Genova, Danilo, Kolzenburg S, Wiesmaier S, Dallanave E, Neuville DR, Kai-Uwe Hess, Dingwell DB (2017) A compositional tipping point governing the mobilization and eruption style of rhyolitic magma. Nature 552(7684):235–238
- Donnelly-Nolan JM, Stovall WK, Ramsey DW, Ewert JW, Jensen RA (2011) Newberry Volcano—central Oregon's sleeping giant. US Geol Surv Fact Sheet 3145(6)
- Druitt TH, Young SR, Baptie B, Bonadonna C, Calder ES, Clarke AB, Cole PD, Harford CL, Herd RA, Luckett R, Ryan G (2002) Episodes of cyclic Vulcanian explosive activity with fountain collapse at Soufrière Hills Volcano, Montserrat. Memoirs-Geol Soc London 21:281–306
- Dufek J, Manga M, Patel A (2012) Granular disruption during explosive volcanic eruptions. Nat Geosci 5(8):561–564
- Eichelberger JC, Carrigan CR, Westrich HR, Price RH (1986) Nonexplosive silicic volcanism. Nature 323(6089):598–602
- Engwell SL, Sparks RSJ, Aspinall WP (2013) Quantifying uncertainties in the measurement of tephra fall thickness. J Appl Volcanol 2(1):1–12. https://doi.org/10.1186/2191-5040-2-5
- Ewert JW (2007) System for ranking relative threats of US volcanoes. Nat Hazard Rev 8(4):112–124
- Ewert JW, Diefenbach AK, Ramsey DW (2018) 2018 update to the US Geological Survey national volcanic threat assessment (No. 2018–5140). US Geological Survey
- Fink JH, Pollard DD (1983) Structural evidence for dikes beneath silicic domes, Medicine Lake Highland Volcano. Calif Geol 11(8):458–461
- Forte P, Castro JM (2019) H2O-content and temperature limit the explosive potential of rhyolite magma during Plinian eruptions. Earth Planet Sci Lett 506:157–167. https://doi.org/10.1016/j.epsl.2018.10.041
- Gardner JE, Carey S, Sigurdsson H (1998) Plinian eruptions at Glacier Peak and Newberry volcanoes, United States: implications for volcanic hazards in the Cascade Range. Geol Soc Am Bull 110(2):173–187
- Gardner JE, Llewellin EW, Watkins JM, Befus KS (2017) Formation of obsidian pyroclasts by sintering of ash particles in the volcanic conduit. Earth Planet Sci Lett 459:252–263
- Gardner JE, Thomas RM, Jaupart C, Tait S (1996) Fragmentation of magma during Plinian volcanic eruptions. Bulletin of Volcanology 58(2–3):144–162
- Giachetti T, Druitt TH, Burgisser A, Arbaret L, Galven C (2010) Bubble nucleation, growth and coalescence during the 1997 Vulcanian explosions of Soufrière Hills Volcano, Montserrat. J Volcanol Geoth Res 193(3–4):215–231
- Giachetti T, Hudak MR, Shea T, Bindeman IN, Hoxsie EC (2020) D/H ratios and H2O contents record degassing and rehydration history of rhyolitic magma and pyroclasts. Earth Planet Sci Lett 530:115909
- Giachetti T, Trafton KR, Wiejaczka J, Gardner JE, Watkins JM, Shea T, Wright HM (2021) The products of primary magma fragmentation finally revealed by pumice agglomerates. Geology 49(11):1307–1311
- Gonnermann HM, Manga M (2007) The fluid mechanics inside a volcano. Annu Rev Fluid Mech 39:321–356
- Heath BA, Hooft EE, Toomey DR, Bezada MJ (2015) Imaging the magmatic system of Newberry Volcano using joint active source and teleseismic tomography. Geochem Geophys Geosyst 16(12):4433–4448
- Houghton BF, Wilson CJN (1989) A vesicularity index for pyroclastic deposits. Bull Volcanol 51(6):451–462
- Janebo MH, Houghton BF, Thordarson T, Bonadonna C, Carey RJ (2018) Total grain-size distribution of four subplinian–Plinian tephras from Hekla volcano, Iceland: Implications for sedimentation dynamics and eruption source parameters. J Volcanol Geoth Res 357:25–38



Bulletin of Volcanology (2022) 84:104 Page 17 of 18 104

Jaupart C, Allègre CJ (1991) Gas content, eruption rate and instabilities of eruption regime in silicic volcanoes. Earth Planet Sci Lett 102(3–4):413–429

- Jensen R, Donnelly Nolan J, Mckay D (2009) A field guide to Newberry Volcano, Oregon, in Volcanoes to Vineyards: Geologic Field Trips Through the Dynamic Landscape of the Pacific Northwest, Field Guide, vol. 15, pp. 53–79, Geol Soc of Am Boulder, Colo. https://doi.org/10.1130/2009.fld015(03)
- Jones TJ, Russell JK (2017) Ash production by attrition in volcanic conduits and plumes. Sci Rep 7(1):1–12
- Jordan BT, Grunder AL, Duncan RA, Deino AL (2004) Geochronology of age-progressive volcanism of the Oregon High Lava Plains: implications for the plume interpretation of Yellowstone. J Geophys Res Solid Earth 109(B10)
- Kansal AR, Torquato S, Stillinger FH (2002) Computer generation of dense polydisperse sphere packings. J Chem Phys 117(18):8212–8218
- Kennedy BM, Spieler O, Scheu B, Kueppers U, Taddeucci J, Dingwell DB (2005) Conduit implosion during Vulcanian eruptions Geology 33(7):581–584
- Klawonn M, Houghton BF, Swanson DA, Fagents SA, Wessel P, Wolfe CJ (2014) Constraining explosive volcanism: subjective choices during estimates of eruption magnitude. Bull Volcanol 76(2):1–6. https://doi.org/10.1007/s00445-013-0793-3
- Klawonn M, Houghton BF, Swanson DA, Fagents SA, Wessel P, Wolfe CJ (2014) From field data to volumes: constraining uncertainties in pyroclastic eruption parameters. Bull Volcanol 76(7):1–16. https://doi.org/10.1007/s00445-014-0839-1
- Klug C, Cashman KV, Bacon C (2002) Structure and physical characteristics of pumice from the climactic eruption of Mount Mazama (Crater Lake), Oregon. Bull Volcanol 64(7):486–501
- Kuehn SC (2002) Stratigraphy, distribution, and geochemistry of the Newberry Volcano tephras. PhD thesis. Washington State University.
- Kuehn SC, Foit FF Jr (2006) Correlation of widespread Holocene and Pleistocene tephra layers from Newberry Volcano, Oregon, USA, using glass compositions and numerical analysis. Quatern Int 148(1):113–137
- LaRue A, Baker DR, Polacci M, Allard P, Sodini N (2013) Can vesicle size distributions assess eruption intensity during volcanic activity? Solid Earth 4(2):373–380
- Le Pennec J-L, Ruiz GA, Ramon P, Palacios E, Mothes P, Yepes H (2012) Impact of tephra falls on Andean communities: the influences of eruption size and weather conditions during the 1999–2001 activity of Tungurahua volcano, Ecuador. J Volcanol Geotherm Res 217–218:91–103
- Macleod NS, Sherrod DR (1988) Geologic evidence for a magma chamber beneath Newberry Volcano, Oregon. Journal of Geophysical Research 93(89):10067–10079.
- MacLeod NS, Sherrod DR, Chitwood LA, Jensen RA (1995) Geologic map of Newberry Volcano, Deschutes, Kalamath, and Lake Counties, Oregon: U.S. Geological Survey Miscellaneous Geologic Investigations Map I-2455, scales 1:62,5000 and 1:24,000
- Miwa T, Iriyama Y, Nagai M, Nanayama F (2020) Sedimentation process of ashfall during a Vulcanian eruption as revealed by high-temporal-resolution grain size analysis and high-speed camera imaging. Prog Earth Planet Sci 7(1):1–16
- Mueller S, Scheu B, Kueppers U, Spieler O, Richard D, Dingwell DB (2011) The porosity of pyroclasts as an indicator of volcanic explosivity. J Volcanol Geoth Res 203(3–4):168–174
- Nguyen CT, Gonnermann HM, Houghton BF (2014) Explosive to effusive transition during the largest volcanic eruption of the 20th century (Novarupta 1912, Alaska). Geology 42(8):703–706

- Ogburn SE, Loughlin SC, Calder ES (2015) The association of lava dome growth with major explosive activity (VEI≥ 4): DomeHaz, a global dataset. Bull Volcanol 77(5):1–17
- Ohashi M, Ichihara M, Kennedy B, Gravley D (2021) Comparison of bubble shape model results with textural analysis: implications for the velocity profile across a volcanic conduit. J Geophys Res Solid Earth e2021JB021841
- Paisley R, Berlo K, Ghaleb B, Tuffen H (2019) Geochemical constraints on the role of tuffisite veins in degassing at the 2008–09 Chaitén and 2011–12 Cordón Caulle rhyolite eruptions. J Volcanol Geoth Res 380:80–93
- Palladino DM, Simei S, Kyriakopoulos K (2008) On magma fragmentation by conduit shear stress: evidence from the Kos Plateau Tuff, Aegean Volcanic Arc. J Volcanol Geoth Res 178(4):807–817
- Pistolesi M, Cioni R, Bonadonna C, Elissondo M, Baumann V, Bertagnini A, Francalanci L (2015) Complex dynamics of small-moderate volcanic events: the example of the 2011 rhyolitic Cordón Caulle eruption, Chile. Bull Volcanol 77(1):1–24
- Popa RG, Bachmann O, Huber C (2021) Explosive or effusive style of volcanic eruption determined by magma storage conditions. Nat Geosci 14(10):781–786
- Ruprecht P, Bachmann O (2010) Pre-eruptive reheating during magma mixing at Quizapu volcano and the implications for the explosiveness of silicic arc volcanoes. Geology 38(10):919–922
- Rust AC, Cashman KV (2007) Multiple origins of obsidian pyroclasts and implications for changes in the dynamics of the 1300 BP eruption of Newberry Volcano, USA. Bull Volcanol 69(8):825–845
- Saubin E, Tuffen H, Gurioli L, Owen J, Castro JM, Berlo K, McGowan EM, Schipper CI, Wehbe K (2016) Conduit dynamics in transitional rhyolitic activity recorded by tuffisite vein textures from the 2008-2009 Chaitén Eruption. Front Earth Sci 4. https://doi.org/10.3389/feart.2016.00059
- Saxby J, Rust A, Beckett F, Cashman K, Rodger H (2020) Estimating the 3D shape of volcanic ash to better understand sedimentation processes and improve atmospheric dispersion modelling. Earth Planet Sci Lett 534
- Scandone R, Cashman KV, Malone SD (2007) Magma supply, magma ascent and the style of volcanic eruptions. Earth Planet Sci Lett 253(3–4):513–529
- Schipper CI, Castro JM, Tuffen H, James MR, How P (2013) Shallow vent architecture during hybrid explosive–effusive activity at Cordón Caulle (Chile, 2011–12): evidence from direct observations and pyroclast textures. J Volcanol Geoth Res 262:25–37
- Schipper CI, Castro JM, Kennedy BM, Tuffen H, Whattam J, Wadsworth FB, Alloway BV (2021) Silicic conduits as supersized tuffisites: clastogenic influences on shifting eruption styles at Cordón Caulle volcano (Chile). Bull Volcanol 83(2):1–22
- Shea T, Houghton BF, Gurioli L, Cashman KV, Hammer JE, Hobden BJ (2010) Textural studies of vesicles in volcanic rocks: an integrated methodology. J Vol Geotherm Res 190:271–289
- Sherrod DR (1997) Volcano hazards at Newberry volcano, Oregon (pp. 97–513). The survey
- Sherrod DR, MacLeod NS (1979) The last eruptions at Newberry Volcano, central Oregon. In Geol Soc Am Abstr Programs 11(3):127
- Sieh K, Bursik M (1986) Most recent eruption of the Mono Craters, eastern central California. J Geophys Res Solid Earth 91(B12):12539–12571
- Silva Parejas C, Lara LE, Bertin D, Amigo A, Orozco G (2012) The 2011–2012 eruption of Cordón Caulle volcano (Southern Andes): evolution, crisis management and current hazards. In EGU General Assembly Conference Abstracts (p. 9382)
- Sparks RSJ, Melnik O (1999) Nonlinear dynamics of lava dome extrusion. Nature 402:37–41



104 Page 18 of 18 Bulletin of Volcanology (2022) 84:104

Spieler O, Kennedy B, Kueppers U, Dingwell DB, Scheu B, Taddeucci J (2004) The fragmentation threshold of pyroclastic rocks. Earth Planet Sci Lett 226(1–2):139–148

- Stasusik M, Barclay J, Carroll MR, Jaupart C, Ratté JC, Sparks S, Tait S (1996) Degassing during magma ascent in the Mule Creek vent (USA). Bull Volcanol 58(2):117–130. https://doi.org/10.1007/s004450050130
- Taddeucci J, Wohletz KH (2001) Temporal evolution of the Minoan eruption (Santorini, Greece), as recorded by its Plinian fall deposit and interlayered ash flow beds. J Volcanol Geoth Res 109(4):299–317
- Till CB, Grove TL, Carlson RW, Donnelly-Nolan JM, Fouch MJ, Wagner LS, Hart WK (2013) Depths and temperatures of < 10.5 Ma mantle melting and the lithosphere-asthenosphere boundary below southern Oregon and northern California. Geochem Geophys Geosyst 14(4):864–879
- Trafton KR, Giachetti T (2021) The morphology and texture of Plinian pyroclasts reflect their lateral sourcing in the conduit. Earth Planet Sci Lett 562:116844
- Tuffen H, Dingwell DB, Pinkerton H (2003) Repeated fracture and healing of silicic magma generate flow banding and earthquakes? Geology 31:1089–1092
- Wadsworth FB, Llewellin EW, Vasseur J, Gardner JE, Tuffen H (2020) Explosive-effusive volcanic eruption transitions caused by sintering. Sci Adv 6(39):eaba7940
- Walker GP (1973) Explosive volcanic eruptions—a new classification scheme. Geol Rundsch 62(2):431–446

- Walker GW, MacLeod NS (1991) Geologic map of Oregon: Reston, Va., U.S. Geological Survey, scale 1:500,000
- Watkins JM, Gardner JE, Befus KS (2017) Nonequilibrium degassing, regassing, and vapor fluxing in magmatic feeder systems. Geology 45(2):183–186
- Wearn KM (2002) Obsidian pyroclast from the Cleetwood and Rock Mesa eruptions, Central Oregon. MSc thesis, University of Oregon, Eugene
- Wicks C, de La Llera JC, Lara LE, Lowenstern J (2011) The role of dyking and fault control in the rapid onset of eruption at Chaitén volcano, Chile. Nature 478(7369):374–377
- Wiejaczka J, Giachetti T (2022) Using eruption source parameters and high-resolution grain-size distributions of the 7.7 ka Cleetwood Eruption of Mount Mazama (Oregon, United States) to reveal primary and secondary eruptive processes. Front Earth Sci 460
- Wright HM, Cashman KV, Rosi M, Cioni R (2007) Breadcrust bombs as indicators of Vulcanian eruption dynamics at Guagua Pichincha volcano, Ecuador. Bull Volcanol 69(3):281–300
- Xue M, Allen RM (2006) Origin of the Newberry Hotspot Track: evidence from shear-wave splitting. Earth Planet Sci Lett 244(1-2):315-322

Springer Nature or its licensor (e.g. a society or other partner) holds exclusive rights to this article under a publishing agreement with the author(s) or other rightsholder(s); author self-archiving of the accepted manuscript version of this article is solely governed by the terms of such publishing agreement and applicable law.

